A: Spectroscopy, Molecular Structure, and Quantum Chemistry

A Variationally Computed IR Line List for the Methyl Radical CH

Ahmad Y. Adam, Andrey Yachmenev, Sergei N. Yurchenko, and Per Jensen

Just Accepted

A Variationally Computed IR Line List for the

Methyl Radical CH$_3$

Ahmad Y. Adam,[†] Andrey Yachmenev,[‡] Sergei N. Yurchenko,[¶] and Per Jensen[*,†]

[†]*Fakultät für Mathematik und Naturwissenschaften, Physikalische und Theoretische*
Chemie, Bergische Universität Wuppertal, D–42097 Wuppertal, Germany

[‡]*Center for Free-Electron Laser Science, Deutsches Elektronen-Synchrotron DESY,*
Notkestraße 85, D-22607 Hamburg, Germany, The Hamburg Center for Ultrafast Imaging,
Universität Hamburg, Luruper Chaussee 149, D-22761 Hamburg, Germany

[¶]*Department of Physics and Astronomy, University College London, Gower Street, London*
WC1E 6BT, United Kingdom

E-mail: jensen@uni-wuppertal.de

Abstract

We present the first variational calculation of a hot temperature *ab initio* line list for the CH_3 radical. It is based on a high level *ab initio* potential energy surface and dipole moment surface of CH_3 in the ground electronic state. The ro-vibrational energy levels and Einstein A coefficients were calculated using the general-molecule variational approach implemented in the computer program TROVE. Vibrational energies and vibrational intensities are found to be in very good agreement with the available experimental data. The line list comprises 9,127,123 ro-vibrational states ($J \leq 40$) and 2,058,655,166 transitions covering the wavenumber range up to 10000 cm^{-1} and should be suitable for temperatures up to $T = 1500$ K.

Introduction

The methyl radical CH_3 is a free radical of major importance in many areas of science such as hydrocarbon combustion processes,[1] atmospheric chemistry,[2] the chemistry of semiconductor production,[3] the chemical vapor deposition of diamond,[4] and many chemical processes of current industrial and environmental interest. It is also expected to be present in exo-planetary atmospheres,[5] in the atmospheres of Saturn[6] and Neptune,[7] and in the interstellar medium,[8] where it is thought to be one of the most abundant free radicals.[5] Because of its central role in this variety of situations, its structural and spectroscopic parameters have been extensively studied. Diverse spectroscopic techniques have been employed to determine absolute concentrations of CH_3 in the gas phase, including UV/visible,[9] infrared,[10] and Raman spectroscopies.[11–17] In addition, CH_3 is an example of a molecule with large vibrational contribution to the hyperfine coupling constant, accounting for up to about 41% of the total value (see Ref. 18 and references therein).

Owing to the importance of CH_3 in various contexts, in particular in astrophysics and -chemistry, its concentrations or column densities in remote environments such as interstellar space, the terrestrial atmosphere, exo-planetary atmospheres, and the outer layers of cool

28 stars are of interest and it is desirable to determine these by remote-sensing spectroscopic

29 methods. A prerequisite for such determinations is the knowledge of the transition moments

30 for the observed transitions, and these must often be obtained in theoretical calculations

31 as done, for example, in the ExoMol project[19,20] by Yurchenko and co-workers.[21–33] This

32 project aims at providing theoretically computed transition moments and simulated spectra

33 for (small to medium-sized) general polyatomic molecules of astrophysical and/or -chemical

34 interest. In general, molecular transition moments known to within 10-20% (the typical

35 accuracy of the transition moment data of the HITRAN database[34]) are sufficiently accurate

36 to be useful for most applications involving determination of concentrations and column

37 densities, at least for fundamental and overtone bands. The level of ab $initio$ theory used in

38 the present study [RCCSD(T)-F12b /cc-pVQZ-F12; see below] is expected to be sufficient

39 to satisfy this requirement for the transition moments computed in the present work. Also,

40 we expect the inaccuracy of our calculations to be predominantly caused by the inaccuracy

41 of the ab $initio$ potential energy surface, and not by the truncation of the kinetic energy

42 operator expansion.

43 　　At equilibrium, the three protons of electronic-ground-state $\tilde{X}$ $^2A_2''$ CH_3 form an equi-

44 lateral triangle with the C nucleus at the centre-of-mass of the planar structure with $\boldsymbol{D}_{3h}$

45 point group symmetry (see Table A-10 of Ref. 35). There is no permanent dipole mo-

46 ment, and so the pure rotational transitions are dipole forbidden and very weak. Also, the

47 planar ground-state equilibrium structure precludes most one-photon transitions to excited

48 electronic states.[36] Owing to the extremely weak rotational spectrum, determinations of

49 concentrations and column densities for CH_3 must be made with rovibrational transitions in

50 the infrared region. The most suitable transitions are those in the intense ν_2 fundamental

51 band at 606 cm^{-1} (where ν_2 is the out-of-plane bending mode). This band provides con-

52 venient transitions for concentration measurements and has been used extensively for this

53 purpose.[37–40] As mentioned above, the corresponding transition moments must be known

54 in order that concentrations can be determined, and the present work can be viewed as a

55 first step towards providing extensive catalogues of theoretical transition moments for CH_3,

56 so-called line lists, of use in astrophysical studies. In the present work we apply a high

57 level *ab initio* potential energy surface, refined by means of experimental spectroscopic data,

58 and *ab initio* dipole moment surfaces to compute, with the TROVE program,[41–44] sufficient

59 energies and transition moments for generating a hot ($T = 1500$ K) IR line list for CH_3.

Theory

Potential energy surface

62 The potential energy surface (PES) employed for the electronic ground state of CH_3 in the

63 present work is based on the *ab initio* surface reported in Ref. 18, which we denote as

64 PES-1. The PES-1 electronic energies were computed for $24\,000$ symmetry-unique molecu-

65 lar geometries at the open-shell RCCSD(T)-F12b[45,46] level of theory (explicitly correlated

66 F12 restricted coupled cluster included single and double excitations with a noniterative

67 correction for triples) and the F12-optimized correlation consistent polarized valence basis

68 set cc-pVQZ-F12.[47] The carbon inner-shell electron pair was treated as frozen core in the

69 correlated calculations. By using the frozen-core approximation we benefit from error can-

70 cellation. It is well known that, e.g. for second-row atoms, the core-valence correlation is

71 almost exactly cancelled by the more costly high-order correlation effects.[48] Keeping only

72 one of them would make the accuracy deteriorate.

73 The analytical representation for the PES was obtained in a least-squares fitting proce-

74 dure using the parameterized function from Lin *et al.*[49]:

$$V(\xi_1, \xi_2, \xi_3, \xi_{4a}, \xi_{4b}; \sin \bar{\rho}) = V_e + V_0(\sin \bar{\rho}) + \sum_j F_j(\sin \bar{\rho}) \, \xi_j$$

$$+ \sum_{j \leqslant k} F_{jk}(\sin \bar{\rho}) \, \xi_j \, \xi_k + \sum_{j \leqslant k \leqslant l} F_{jkl}(\sin \bar{\rho}) \, \xi_j \, \xi_k \, \xi_l$$

$$+ \sum_{j \leqslant k \leqslant l \leqslant m} F_{jklm}(\sin \bar{\rho}) \, \xi_j \, \xi_k \, \xi_l \, \xi_m + \ldots; \tag{1}$$

this function depends on the stretching variables

$$\xi_k = 1 - \exp\left[-a(r_k - r_e)\right], \quad k = 1, 2, 3, \tag{2}$$

where r_k is the instantaneous value of the distance between the C nucleus and the proton H_k labeled $k = 1$, 2, or 3; r_e is the common equilibrium value of the three r_k bond lengths, and a is a Morse parameter. Furthermore, the symmetrized bending variables (ξ_{4a}, ξ_{4b}) are defined as

$$(\xi_{4a}, \xi_{4b}) = \left(\frac{1}{\sqrt{6}}[2\,\alpha_1 - \alpha_2 - \alpha_3], \frac{1}{\sqrt{2}}[\alpha_2 - \alpha_3] \right) \tag{3}$$

with α_i as the bond angle $\angle(H_j X H_k)$ where (i, j, k) is a permutation of the numbers (1,2,3). Finally, the variable

$$\sin \bar{\rho} = \frac{2}{\sqrt{3}} \sin[(\alpha_1 + \alpha_2 + \alpha_3)/6] \tag{4}$$

75 describes the out-of-plane bending. At the planar equilibrium configuration, we have $\alpha_1 +$

76 $\alpha_2 + \alpha_3 = 360°$ and so $\sin \bar{\rho} = \sin \bar{\rho}_e = 1$. The functions $V_0(\sin \bar{\rho})$ and $F_{jk\ldots}(\sin \bar{\rho})$ in Eq. (1)

77 are defined as

$$V_0(\sin \bar{\rho}) = \sum_{s=1}^{4} f_0^{(s)} \, (1 - \sin \bar{\rho})^s, \tag{5}$$

$$F_{jk\ldots}(\sin \bar{\rho}) = \sum_{s=0}^{N} f_{jk\ldots}^{(s)} \, (1 - \sin \bar{\rho})^s, \tag{6}$$

78 where the quantities $f_0^{(s)}$ and $f_{jk\ldots}^{(s)}$ in Eqs. (5) and (6) are expansion coefficients. The opti-

79 mized values of the parameters a, r_e, $f_0^{(s)}$, and $f_{jk\ldots}^{(s)}$ are given in the supplementary material

80 to Ref. 18 together with Fortran 90 routine for calculating PES values.

81 The analytical form of PES-1[18] is given in terms of the *ab initio* cc-pVQZ-F12 values

82 of the equilibrium structural parameters, $r_e = 1.0774$ Å and $\alpha_e = 120°$,[18] for the electronic

83 ground state of CH_3. In the present work, we optimized the value of r_e in a least-squares

84 fitting to experimentally derived to rotational energy spacings within the vibrational states

85 of CH_3. The fitting produced $r_e = 1.0763$ Å; $\alpha_e = 120°$ by symmetry. We use these optimized

86 values of the equilibrium structural parameters. All results presented below are based on the

87 analytical potential energy function called PES-2, obtained from PES-1[18] by replacing the

88 *ab initio* cc-pVQZ-F12 value of r_e by the adjusted value given here. The remaining PES-2

89 parameter values are identical to those of PES-1 and can be obtained from the supplementary

90 material to Ref. 18.

91 Dipole moment surface

92 The dipole moment surface (DMS) for the electronic ground state of CH_3 was computed

93 using the MOLPRO[50] program package. Frozen-core calculations were carried out for $19\,361$

94 symmetry-unique geometries ($15\,600$ below $30\,000$ cm^{-1}) using the spin-restricted open-shell

95 coupled cluster theory RCCSD(T)[51] and the augmented correlation consistent valence ba-

96 sis set aug-cc-pVTZ,[52,53] employing the two-point stencil central finite differences with the

97 electric field strength of 0.002 a.u.

We employ the so-called symmetrized molecular-bond (SMB) representation[22] [which is

an extension of the molecular-bond (MB) representation[54]] to formulate analytical functions

describing the molecular dipole moment components. The SMB representation makes use

of the projections $\bar{\boldsymbol{\mu}} \cdot \mathbf{e}_k$ of the dipole moment on the molecular bonds, where $\mathbf{e}_k$ is the unit

vector along the C–H_k bond,

$$\mathbf{e}_k = \frac{\mathbf{r}_k - \mathbf{r}_4}{|\mathbf{r}_k - \mathbf{r}_4|} \tag{7}$$

98   with $\mathbf{r}_k$, $k = 1, 2, 3$, as the position vector of proton k and $\mathbf{r}_4$ as the position vector of the

99   C nucleus.

100   We form symmetry-adapted linear combinations of the MB projections $\bar{\boldsymbol{\mu}} \cdot \mathbf{e}_j$:

$$\bar{\mu}_{A_2''}^{\mathrm{SMB}} = (\bar{\boldsymbol{\mu}} \cdot \mathbf{e}_{\mathrm{N}}) \tag{8}$$

$$\bar{\mu}_{E_a'}^{\mathrm{SMB}} = \frac{1}{\sqrt{6}} [2 (\bar{\boldsymbol{\mu}} \cdot \mathbf{e}_1) - (\bar{\boldsymbol{\mu}} \cdot \mathbf{e}_2) - (\bar{\boldsymbol{\mu}} \cdot \mathbf{e}_3)] \tag{9}$$

$$\bar{\mu}_{E_b'}^{\mathrm{SMB}} = \frac{1}{\sqrt{2}} [(\bar{\boldsymbol{\mu}} \cdot \mathbf{e}_2) - (\bar{\boldsymbol{\mu}} \cdot \mathbf{e}_3)], \tag{10}$$

where, in addition to the vectors $\mathbf{e}_k$, we have introduced $\mathbf{e}_{\mathrm{N}} = \mathbf{q}_{\mathrm{N}}/|\mathbf{q}_{\mathrm{N}}|$ with $\mathbf{q}_{\mathrm{N}}$ as the 'trisector'

$$\mathbf{q}_{\mathrm{N}} = (\mathbf{e}_1 \times \mathbf{e}_2) + (\mathbf{e}_2 \times \mathbf{e}_3) + (\mathbf{e}_3 \times \mathbf{e}_1). \tag{11}$$

101   The subscripts $\Gamma = A_2''$, E_a', and E_b' of the quantities $\bar{\mu}_\Gamma^{\mathrm{SMB}}$ in Eqs. (8)–(10) refer to the

102   irreducible representations (Table A-10 of Ref. 35) of the CH_3 molecular symmetry group

103   $\boldsymbol{D}_{3h}(\mathrm{M})$; the electronically averaged dipole moment $\bar{\boldsymbol{\mu}}$ generates the representation $A_2'' \oplus$

104   E'. The quantity $\bar{\mu}_{A_2''}^{\mathrm{SMB}}$ is antisymmetric under the inversion operation[35] E^* and vanishes

105   at planarity, so that $\bar{\boldsymbol{\mu}}$ has only two non-vanishing, linearly independent components at

106   planarity. These two components vanish at planar configurations with $\boldsymbol{D}_{3h}$ point group

107   symmetry.

The three components of the SMB dipole moment in Eqs. (8)–(10) are represented by 4th order polynomial expansions

$$\bar{\mu}_\Gamma^{\mathrm{SMB}}(\chi_1, \chi_2, \chi_3, \chi_{4a}, \chi_{4b}; \rho) = \mu_0^\Gamma (\sin \bar{\rho}) + \sum_i \mu_i^\Gamma (\sin \bar{\rho}) \chi_i + \sum_{i \le j} \mu_{ij}^\Gamma (\sin \bar{\rho}) \chi_i \chi_j$$
$$+ \sum_{i \le j \le k} \mu_{ijk}^\Gamma (\sin \bar{\rho}) \chi_i \chi_j \chi_k + \sum_{i \le j \le k \le l} \mu_{ijkl}^\Gamma (\sin \bar{\rho}) \chi_i \chi_j \chi_k \chi_l, \tag{12}$$

in terms of the variables

$$\chi_k = \Delta r_k (1 - \exp(-\Delta r_k))^2, \quad (k = 1, 2, 3) \tag{13}$$

with $\Delta r_k = r_k - r_{\mathrm{e}}$ and

$$(\chi_4, \chi_5) = (\xi_{4a}, \xi_{4b}) \tag{14}$$

where (ξ_{4a}, ξ_{4b}) are defined in Eq. (3). The expansion coefficients $\mu_{ij\ldots}^{\Gamma}(\sin \bar{\rho})$ are defined as

$$\mu_{ij\ldots}^{\Gamma}(\sin \bar{\rho}) = \sum_{s=0}^{N} \mu_{ij\ldots}^{\Gamma(s)}(1 - \sin \bar{\rho})^s, \tag{15}$$

108 where $\sin \bar{\rho}$ is given by Eq. (4) and the maximal order of the polynomial is $N = 8$. For more

109 details the reader is referred to Ref. 22. The final fit of the 15 600 geometries required a total

110 number of 218 parameters (131 for $\bar{\mu}_{A_2''}^{\mathrm{SMB}}$ and 87 for $\bar{\mu}_{E_a'}^{\mathrm{SMB}}$ and $\bar{\mu}_{E_b'}^{\mathrm{SMB}}$) and reproduced the

111 *ab initio* data with a root-mean-square (RMS) differences of 0.003 D, 0.001 D and 0.004 D

112 for the x, y and z components respectively and energies up to 30 000 cm^{-1}, see Figure 1. A

113 series of fittings to the x, y and z *ab initio* dipole-moment components have been carried

114 out, including in the data set for each fitting the *ab initio* points with electronic energy

115 (relative to the potential energy minimum) $V \leqslant E$, and increasing E. Figure 1 shows the

116 RMS deviation for each dipole-moment component as a function of E. The DMS expansion

117 parameter set and the Fortran 90 functions are included in the supplementary material.

Intensity simulations with TROVE

119 The 'readiness' of the molecule to make an absorption or emission transition from an initial

120 ro-vibrational state i to a final ro-vibrational state f is expressed by the line strength[35,55,56]

121 $S(f \leftarrow i)$, a quantity with units of [dipole moment]^2 (typically Debye^2). For $S(f \leftarrow i) =$

122 0, the transition does not take place and need not be considered. As discussed in Ref. 35

123 transitions with $S(f \leftarrow i) \neq 0$ are said to satisfy selection rules which we can derive from

124 symmetry considerations before we do quantitative, numerical calculations of $S(f \leftarrow i)$.

125 Thus, these calculations need only be done for transitions satisfying the selection rules, and

126 after obtaining values of $S(f \leftarrow i)$ for these transitions, we can compute the corresponding

127 Einstein coefficients and absorption intensities.

Figure 1: Root-mean-square (RMS) errors of the fittings to the *ab initio* dipole moment values. The results of a series of fittings are shown. In each fitting, the data set includes the *ab initio* points with electronic energy (relative to the potential energy minimum) $V \leqslant E$ (see text).
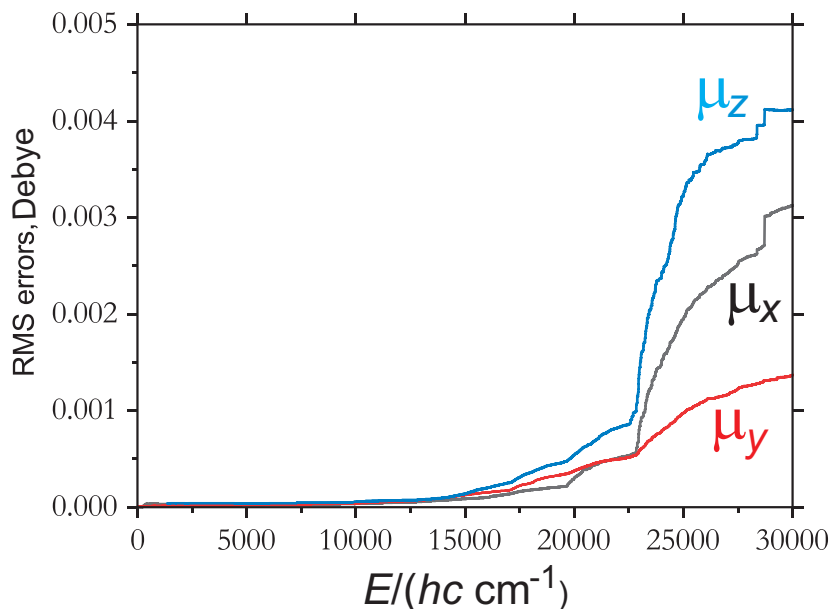
The initial(final) state $i(f)$ has the rotation-vibration wavefunction $|\Phi_{\mathrm{rv}}^{(i)}\rangle(|\Phi_{\mathrm{rv}}^{(f)}\rangle)$. The line strength[35,55,56] $S(f \leftarrow i)$ of the ro-vibrational transition $f \leftarrow i$ is

$$S(f \leftarrow i) = g_{\mathrm{ns}} \sum_{M_f, M_i} \sum_{A=X,Y,Z} \left| \left\langle \Phi_{\mathrm{rv}}^{(f)} \left| \bar{\mu}_A \right| \Phi_{\mathrm{rv}}^{(i)} \right\rangle \right|^2, \tag{16}$$

128   where the nuclear spin statistical weight factor[35] is denoted g_{ns} and the electronically aver-

129   aged component of the molecular dipole moment along the space-fixed axis[35] is denoted $\bar{\mu}_A$,

130   $A = X$, Y, or Z. The quantity $M_i(M_f)$ is the quantum number defining the projection of

131   the total angular momentum $\hat{\mathbf{J}}$ on the Z axis for the initial(final) state.

Assuming that the molecules considered are in thermal equilibrium at the absolute tem-

perature T, the intensity of a spectral line is determined as

$$I(f \leftarrow i) = \frac{8\pi^3 N_A \tilde{\nu}_{if}}{(4\pi\epsilon_0)3hc} \frac{\mathrm{e}^{-E_i/kT}}{Q} \left[1 - \exp(-hc\tilde{\nu}_{if}/kT)\right] S(f \leftarrow i). \tag{17}$$

132   Here, the absorption wavenumber is denoted $\tilde{\nu}$, and Eq. (17) yields the intensity of a transi-

133   tion from the initial state i with energy E_i to the final state f with energy E_f, where $hc\tilde{\nu}_{if}$

134   $= E_f - E_i$. The partition function Q is defined as $Q = \sum_j g_j \exp(-E_j/kT)$, where g_j is the

135   total degeneracy of the state with energy E_j and the sum runs over all energy levels of the

136   molecule, and other symbols have their usual meanings. The total degeneracy g_j is given

137   by $(2J + 1)$ times the spin degeneracy $(2S + 1 = 2)$ and times the nuclear spin degeneracy

138   which is 4, 0, 2, 4, 0, 2 for A_1', A_2', E', A_1'', A_2'', and E'' symmetries respectively. The ground

139   electronic state of CH_3 is a doublet ($\tilde{X}\ ^2A_2''$) with a small splitting[57,58] in the rovibrational

140   energy levels due to spin-rotation interactions, around 0.01 cm^{-1}, which we therefore chose

141   to ignore in the present work.

142   Yurchenko $et\ al.$[55] have given, in their Eq. (21), a detailed expression for the line strength

143   of an individual ro-vibrational transition within an isolated electronic state of an XY_3 pyra-

144   midal molecule. Assuming that the populations of the lower (initial) states are Boltzmann-

145   distributed, we limit the intentity calculations to transitions starting from levels below

146   $E_i^{\mathrm{max}}/hc = 9\,000\ \mathrm{cm}^{-1}$. With this limitation, Boltzmann factors of $\exp(-E_i/kT) > 2 \times 10^{-4}$

147   enter into Eq. (17) for $T = 1500$ K. It is common to use the partition function for estimating

148   the completeness of the line list for a given temperature.[24] Towards this end, we consider the

149   ratio $Q_{9000\,\mathrm{cm}^{-1}}/Q_{\mathrm{total}}$, where Q_{total} is the converged partition function value calculated by

150   explicit summation over all computed energy levels and $Q_{9000\,\mathrm{cm}^{-1}}$ is the partition function

151   value calculated by summation over levels with energies lower than 9000 cm^{-1}. This ratio

152   gives 95 % completeness at temperatures below 1500 K. Consequently, we estimate $T =$

153   1500 K to be the maximal temperature for which our line list is realistic. Since it is safe to

154   limit the lower-state energies to be below 9000 cm^{-1}, it is sufficient to consider rotational

155 states with $J \leqslant 40$. We compute a line list in the wavenumber range 0–10 000 cm^{-1}; the

156 upper energy limit (i.e., the maximum value of the final-state energy) corresponds to a term

157 value of $E^{\mathrm{max}}/hc = 19{,}000$ cm^{-1}.

Computational details

158

159 The variational nuclear-motion calculations are done with a symmetry-adapted basis set.

160 With such a basis set, the Hamiltonian matrix becomes block diagonal according to the

161 irreducible representations of the $\boldsymbol{D}_{3h}(M)$ molecular symmetry group:[35] A_1', A_2', A_1'', A_2'', E',

162 and E''. The A_2' and A_2'' matrices are of no interest for CH_3 as the corresponding states have

163 zero nuclear spin statistical weights and do not exist in nature.[35] The E' and E'' matrices

164 each split into two sub-blocks, of which only one must be diagonalized.[35]

The calculation of the matrix elements $\langle \Phi_{\mathrm{rv}}^{(f)} | \bar{\mu}_A | \Phi_{\mathrm{rv}}^{(i)} \rangle$ in Eq. (16) is the bottle-neck in the

spectrum simulations. Here, the wavefunctions $\Phi_{\mathrm{rv}}^{(w)}$ are given as superpositions of symmetry-

adapted basis functions (see Eq. (65) of Yurchenko $et\ al.$[44]):

$$|\Phi_{\mathrm{rv}}^{(w)}\rangle = \sum_{VK\tau_{\mathrm{rot}}} C_{VK\tau_{\mathrm{rot}}}^{(w)} |J_w\, K\, m_w\, \tau_{\mathrm{rot}}\rangle |V\rangle, \quad w = i \ \mathrm{or} \ f, \tag{18}$$

165 with the $C_{VK\tau_{\mathrm{rot}}}^{(w)}$ as expansion coefficients. In Eq. (18), the symmetrized rotational basis

166 functions are denoted $|J_w\, K\, m_w\, \tau_{\mathrm{rot}}\rangle$ with τ_{rot} (= 0 or 1) defining the rotational parity, and

167 $|V\rangle$ is a vibrational basis function. In order to accelerate this part of the calculation, we

168 pre-screened the expansion coefficients $C_{VK\tau_{\mathrm{rot}}}^{(f)}$. All terms with coefficients less than the

169 threshold value of 10^{-13} were discarded in the intensity calculation.

The evaluation of the dipole moment matrix elements $\langle \Phi_{\mathrm{rv}}^{(f)} | \bar{\mu}_A | \Phi_{\mathrm{rv}}^{(i)} \rangle$ has been made more

efficient in a two-step procedure. In the first step, an effective line strength is evaluated for

a given lower state i:

$$S_{i,VK}^A = \langle \Phi_{\mathrm{rv}}^{(i)} | \bar{\mu}_A | \phi_{VK} \rangle. \tag{19}$$

Here, ϕ_{VK} is a short-hand notation for the primitive basis function $|J_w K\, m_w\, \tau_{\text{rot}}\rangle \times |V\rangle$. From the $S_{i,VK}$-values obtained, we compute, in the second step, the line strength $S(f \leftarrow i)$ as

$$S(f \leftarrow i) = g_{\text{ns}} \sum_{m_i, m_f} \sum_{A=X,Y,Z} \left| \sum_{V,K} C^{(f)}_{VK\tau_{\text{rot}}} S^A_{i,VK} \right|^2. \tag{20}$$

170   We had to compute a very large number of transitions satisfying the selection rule $|J_f - J_i|$

171 $\leqslant 1$, where J_i and J_f are the values of the angular momentum quantum number J for

172 the initial and final state, respectively. Consequently, we saved memory by organizing the

173 calculation of the ro-vibrational eigenstates and the $S(f \leftarrow i)$-values such that at a given

174 time, only eigenvectors for states with two consecutive J-values, J and $J+1$, are available for

175 the computation of $S(f \leftarrow i)$-values. This algorithm is implemented in the GPU GAIN-MPI

176 program.[59]

177   The vibrational basis set $|V\rangle$ is obtained in TROVE using a multi-step contraction and

178 symmetrization procedure, starting from local primitive basis set functions, each depending

179 on one variable only (see Refs. 42–44 and references therein). Thus, a compact representation

180 of the vibrational basis set is obtained in a form optimized for the molecule of interest. The

181 final vibrational basis set is represented by the eigenfunctions of the purely vibrational part

182 of the Hamiltonian; we call these eigenfunctions the '$J = 0$ basis'.

Results

Basis set convergence and empirical adjustment of the vibrational band centers

186 The dimensions of the Hamiltonian matrix blocks to be diagonalized are important in de-

187 termining the accuracy of the computed energies and wavefunctions for highly excited ro-

188 vibrational states. Consequently it is imperative to determine empirically the smallest basis

189 set with which the required eigenvalue accuracy (i.e., the optimum basis-set size for 'conver-

190 gence') can be attained.

In TROVE, the size of the vibrational basis set is controlled by polyad number trunca-

tion.[41–43] For CH_3, the polyad number P is defined as:

$$P = 2(n_1 + n_2 + n_3) + n_4 + n_5 + n_6, \tag{21}$$

191 where n_i are the principal quantum numbers associated with the primitive functions $\phi_{n_i}(\xi_i)$.

192 The primitive vibrational basis functions are products of one-dimensional basis functions

193 $\phi_{n_i}(\xi_i)$, and only products with $P \leq P_{max}$ are included in the primitive vibrational basis.

194 An even tighter level of convergence could be achieved for the vibrational term values

195 if these were calculated with different P_{max}-values and the resulting progression of term

196 values were extrapolated to the complete vibrational basis set limit.[60] However, for the

197 purpose of generating line lists this is not considered necessary. The corrections from the

198 extrapolation will be small compared with the term-value errors caused by the imperfection of

199 the underlying potential energy surface. Instead, we pragmatically aim for a higher accuracy

200 by resorting to an empirical approach: The theoretical vibrational term values are replaced

201 by the available accurate, experimentally derived vibrational band-centre values. In this

202 manner, we are adjusting the vibrational band centers 'manually'; this empirical adjustment

203 also shifts the rotational energy-level structure towards better agreement with experiment.

204 We call this procedure the EBSC scheme as it can be regarded as an Empirical Basis Set

205 Correction.

206 We adopt the EBSC scheme for the vibrational bands ν_2, $2\nu_2$, ν_1, ν_4^1, and ν_3^1, for which

207 accurate experimental data are available, in combination with PES-2, where we have adjusted

208 the equilibrium structure of the molecule to fit the experimentally derived pure rotational

209 term values. The vibrational basis set was truncated at the polyad number $P_{max} = 32$. We

210 incorporate experimental information in the EBSC scheme, and so we obviously depart from

211 a purely *ab initio* approach. This is considered justified by the accuracy improvement that

212 can be achieved in the computation of an extensive ro-vibrational line list.

213   To improve the accuracy of the predicted vibrational band-centers, a more thorough

214 refinement of the PES would be required. However, the available accurate experimental

215 data for the vibrationally excited states of CH_3 is severely limited, and so we opted for the

216 EBSC approach in conjunction with the r_e-refinement. For all bands that are not EBSC-

217 corrected, the predicted vibrational term values are determined to a significant extent by the

218 *ab initio* data, and so their accuracy is limited. However, we have improved the prediction

219 of the rotational structures, and that will facilitate the assignments of future experimental

220 spectra for CH_3.

221   In Table 1, the vibrational term values below 5000 cm^{-1} of the methyl radical, calculated

222 variationally in the present work from PES-2, are compared with the available experimental

223 data. The EBSC substitution was made in the $J > 0$ TROVE calculations of the present

224 work, in that the theoretical vibrational term values (obtained for $P_{\max} = 32$) were replaced

225 by the experimental values in Table 1. This table also shows the effect of the polyad number

226 $P_{\max}$ on the vibrational energy.

227   Table 2 shows a comparison of the pure rotational energies ($J \leq 5$) of CH_3 before and

228 after refinement of r_e illustrating the importance of this step.

    The vibrational transition moments are defined as

$$\mu_{V'V} = \sqrt{\sum_{\alpha=x,y,z} |\langle V' \mid \bar{\mu}_\alpha \mid V\rangle|^2} \tag{22}$$

229 where $|V'\rangle$ and $|V\rangle$ denote $J = 0$ vibrational wavefunctions and $\bar{\mu}_\alpha$ is the electronically-

230 averaged dipole moment in the molecular frame (see the section entitled 'Dipole moment

231 surface' above). For calculation of vibrational transition moments we used our *ab initio*

232 PES-1 and truncated the vibrational basis set at polyad number $P_{\max} = 32$. A number

233 of computed transition moments for the strongest lower lying bands are listed in Table

234 3 where they are compared with the available experimental data. The complete list of

Table 1: **Vibrational band centers (cm^{-1}) of ^{12}CH$_3$ from variational calculations.**

Γ	State	Ref.	Obs.[a]	$P_{\max} = 24$[b]	$P_{\max} = 32$[c]
A_1'	$2\nu_2$	61	1288.1	1279.77	1281.24
	$2\nu_4$			2737.63	2739.64
	$4\nu_2$			2773.65	2776.86
	ν_1	13	3004.42	3002.71	3002.76
	$3\nu_4^3$			4118.59	4120.58
	$\nu_1 + 2\nu_2$			4258.97	4260.53
	$6\nu_2$			4391.99	4397.00
	$\nu_3^1 + \nu_4^1$			4537.94	4538.93
	$4\nu_4$			5371.39	5364.56
	$2\nu_2 + 3\nu_4^3$			5475.84	5480.07
	$4\nu_2 + 2\nu_4$			5601.91	5607.20
E'	ν_4^1	62	1397.0	1385.99	1387.26
	$2\nu_2 + \nu_4^1$			2688.80	2691.61
	$2\nu_4^2$			2759.77	2762.05
	ν_3^1	58	3160.8	3158.88	3158.83
	$3\nu_4^1$			4074.69	4075.46
	$2\nu_2 + 2\nu_4^2$			4087.92	4091.72
A_2''	ν_2	13	606.453	602.43	602.43
	$3\nu_2$			2010.09	2010.09
	$\nu_2 + 2\nu_4^0$			3372.27	3371.59
	$5\nu_2$			3569.96	3569.95
	$\nu_1 + \nu_2$			3596.35	3596.30
	$3\nu_4^3$			4768.70	4767.06
	$\nu_2 + 2\nu_4^0$			4823.32	4822.79
	$\nu_1 + 3\nu_2$			4981.58	4981.52
E''	$\nu_2 + \nu_4^1$			2000.24	2002.22
	$\nu_2 + 2\nu_4^2$			3388.24	3391.11
	$3\nu_2 + \nu_4^1$			3426.45	3430.06
	$\nu_2 + \nu_3^1$			3736.40	3736.97
	$\nu_2 + 3\nu_4^1$			4726.62	4728.62
	$3\nu_2 + 2\nu_4^2$			4835.22	4839.85
	$\nu_1 + \nu_2 + \nu_4^1$			4980.92	4983.16

[a] Experimental values of band centers used to replace the theoretical values $P_{\max} = 32$, see text.

[b] Computed using the $P_{\max} = 24$ basis set in conjunction with PES-2.[18]

[c] Computed using the $P_{\max} = 32$ basis set in conjunction with PES-2.[18]

Table 2: Theoretical rotational term values ($N \leq 5$, in cm^{-1}) of CH$_3$, computed with TROVE using different equilibrium structure parameters.

States			Term values		
N	K	τ_{rot}	Obs.	Obs.-Calc.^{a}	Obs.-Calc.^{b}
1	1	0	14.3189	0.032377	0.004027
2	0	1	57.4396	0.112005	-0.002023
2	2	0	38.1186	0.092340	0.017004
2	1	0	52.6112	0.106875	0.002511
3	3	0	71.3965	0.179934	0.038989
3	2	0	95.5353	0.203902	0.014649
3	1	0	110.0032	0.219365	0.001200
4	0	0	191.2473	0.375024	-0.004034
4	4	0	114.1491	0.295456	0.070301
4	2	0	172.0038	0.353500	0.012772
4	3	0	147.9203	0.327970	0.035289

^{a} Calculated using $r_e = 1.07736927$ Å and $\alpha_e = 120.0°$ (PES-1, see text).

^{b} Calculated using $r_e = 1.0762977119$ Å and $\alpha_e = 120.0°$ (PES-2, see text).

235 theoretical transition moments is given as Supporting Information and can be also found at

236 www.exomol.com.

Intensity simulations

238 The simulation of absorption spectra at a given temperature T and within a particular

239 wavenumber interval requires knowledge of the upper and lower-state energies and the Ein-

240 stein coefficients $A(f \leftarrow i)$ [or the line strengths $S(f \leftarrow i)$; the relationship between $A(f \leftarrow i)$

241 and $S(f \leftarrow i)$ is described in Ref. 55] for all transitions in the chosen wavenumber range. In

242 practice, however, the transitions with intensities below a chosen limit are discarded. The

243 most straightforward presentation of the spectral data is a 'stick' diagram with the stick

244 heights representing the integrated absorption coefficients from Eq. (17). We report here

245 such simulations for the CH$_3$ absorption bands in the wavenumber interval 600–1200 cm^{-1}

246 for the out-of-plane bending mode ν_2. The line strengths in Eq. (17) are computed from

247 Eq. (16) with the spin statistical weights g_{ns} from Ref. 18. The simulations are based on

1
2
3
4
5
6
7
8
9
10
11
12
13
14
15
16
17
18
19
20
21
22
23
24
25
26
27
28
29
30
31
32
33
34
35
36
37
38
39
40
41
42
43
44
45
46
47
48
49
50
51
52
53
54
55
56
57
58
59
60

Table 3: Band Centers ν_{fi} and Vibrational Transition Moments μ_{fi} for CH_3.[a]

States		ν_{fi}/cm^{-1}	Calc. μ_{fi}/D	Obs. μ_{fi}/D	Ref.
f	i				
$2\nu_2$	ν_2	678.81	0.25684	0.31(6)	[40]
ν_2	0	602.43	0.20403	0.215(25)	[37–39]
ν_3^1	0	3158.83	0.03999	0.03(27)	[63,64]
ν_4^1	0	1387.26	0.02931		
$2\nu_3 + \nu_4$	0	4529.74	0.02049		
$\nu_1 + \nu_4^1$	0	4383.56	0.00866		
$2\nu_2 + \nu_3^1$	0	4396.18	0.00486		
$2\nu_3^2$	0	6294.76	0.00462		
$\nu_1 + \nu_3^1$	0	6076.68	0.00321		
$2\nu_4^2$	0	2762.05	0.00313		
$\nu_3^1 + 2\nu_4$	0	5864.94	0.00242		
$3\nu_4^1$	0	4075.46	0.00186		
$2\nu_2 + \nu_3^1 + \nu_4^1$	0	5789.16	0.00130		
$4\nu_2$	0	5856.39	0.00116		

[a] The transitions originate in the vibrational ground state ($i = 0$) with the exception of the hot band $2\nu_2 \leftarrow \nu_2$.

248 PES-2 and the computed DMS described above. The partition-function value used was $Q =$

249 732.734, obtained at 300 K as a summation over all variational term values ($J \leq 40$) below

250 36871.73 cm^{-1}. We have computed 2,058,655,166 transitions using the GPU GAIN-MPI

251 program[59] within the various limits defined above.

252   Figure 2 gives an overview (log-scale) of the absorption spectrum of CH$_3$ at different

253 temperatures produced using the line list (log-scale) by means of the ExoCross program.[65]

254 Figure 3 shows four regions with the strongest, dipole-allowed bands ν_2, ν_4, ν_3 and $\nu_3 + \nu_4$.

Figure 2:   An overview of the absorption spectrum (cross sections) of CH$_3$ at different temperatures $T = 300, 500, 1000$ and 1500 K generated using our line list and the Gaussian line profile with the full-width-at-half-maximum of 1 cm^{-1}.
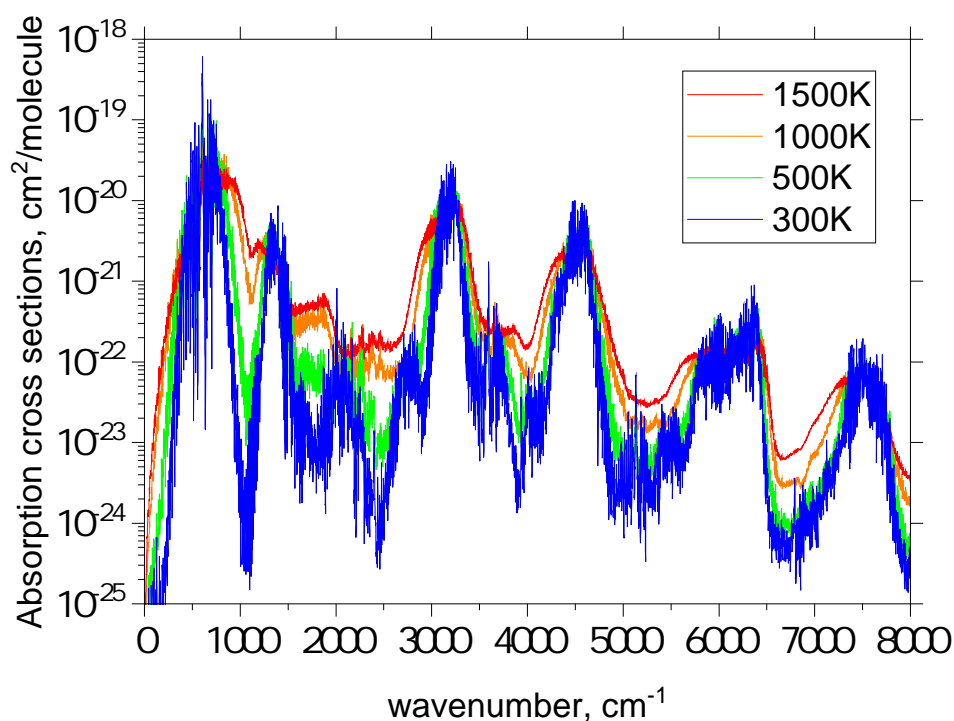
255   Figure 4 shows the emission spectrum of CH$_3$ in the wavenumber interval 600-1200 cm^{-1},

256 simulated with TROVE at two different levels of theory, rovibrational and purely vibrational.

257 The simulated spectra are compared to an experimental spectrum recorded by Hermann and

258 Leone[66,67] (see Fig. 4 of Ref. 66).

Figure 3: A selection of the strongest absorption bands of CH_3 at $T = 296$ K generated using the line list. A Gaussian line profile with the half-width-half-maximum of 0.08 cm^{-1} was used in production of the cross sections shown.
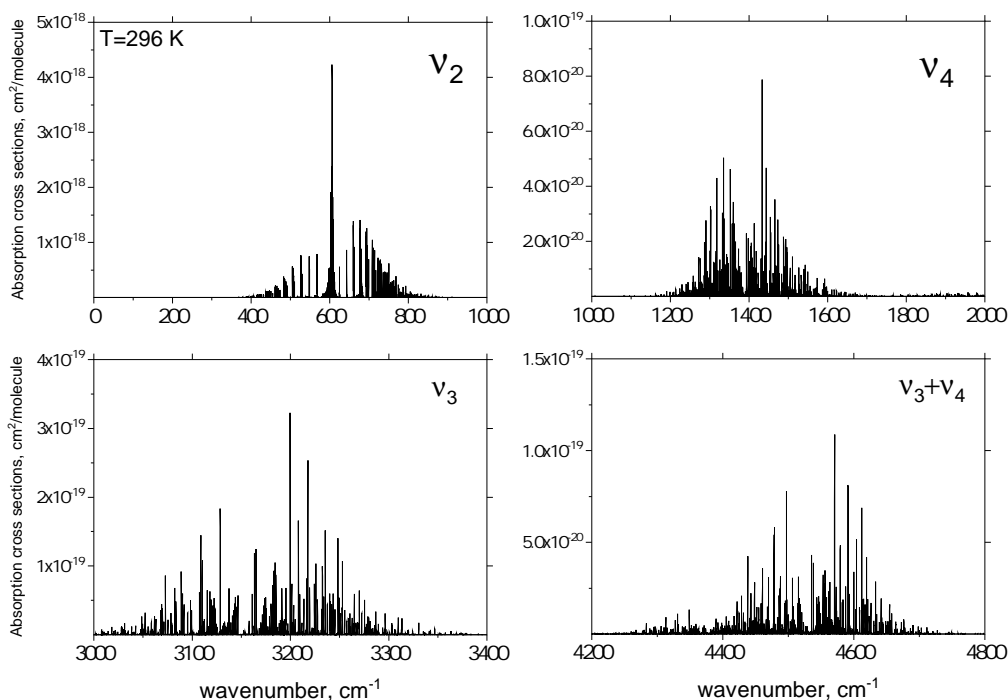
259   Figure 4(a) shows a simulation of the CH_3 emission spectrum, computed with TROVE

260   at a temperature of $T = 300$ K, taking into account all vibrational transitions in the 600-

261   1200 cm^{-1} interval that are calculated with the $P_{max} = 32$ basis set. The simulation involves

262   the convolution of the calculated intensities with a Gaussian line shape function with a full

263   width at half maximum (FWHM) of 17 cm^{-1}.

264   The simulation is compared with the experimental spectrum obtained by Hermann and

265   Leone,[66,67] shown in Figure 4(b).* In the experiment, the CH_3 radicals were produced in

266   a photo-fragmentation process of methyl iodide CH_3I. Hermann and Leone[66,67] suggested

267   that after the breaking of the C–I bond, the CH_3 radicals are predominantly produced in

268   excited states of the out-of-plane bending mode ν_2. The CH_3 fragment of a dissociated

*Reproduced from Hermann, H. W.; Leone, S. R. The Journal of Chemical Physics 1982, 76, 4759–4765, with the permission of AIP Publishing.

269 CH$_3$I molecule will typically have a pyramidal structure close to that of the methyl group

270 in CH$_3$I. For a CH$_3$ radical, however, which is planar at equilibrium, such structures are

271 associated with high excitations of the ν_2 vibrational mode. Excitations with $v_2 \leqslant 10$ have

272 been observed in the emission experiment of Refs. 66,67.

273 In order to simulate vibrationally very hot transitions (hotter than 1500 K) corresponding

274 to the experimental spectrum of Refs. 66 which involves out-of-plane bending states $v_2 \nu_2$

275 with $v_2 \leqslant 10$, we have carried out simulations employing a so-called one-band model (with the

276 one band being the ν_2 fundamental band here). In the one-band model, we use the ν_2-band

277 data from the 'parent', 300 K ro-vibrational line list also for the hot bands accompanying

278 the ν_2 band. The procedure employed is detailed in Ref. 33 and we outline it briefly here:

279 We initially produce the 300 K, ν_2-band cross sections by means of the ExoCross program[65]

280 and convolve them with a Gaussian profile of FWHM $= 17$ cm^{-1} between 0 and 1200 cm^{-1},

281 generating 1201 data points. Then the wavenumbers of the computed cross sections are

282 shifted by -606.4531 cm^{-1}, positioning the band center at zero, and the cross sections

283 are normalized. A local version of ExoCross now obtains, from the vibrational transition

284 moments computed with TROVE, the vibrational band intensities for the hot bands $(v_2+1)\,\nu_2$

285 $\leftarrow v_2\,\nu_2$, $v_2 \leqslant 9$. Finally, the simulated spectrum is generated by placing, for each hot band,

286 the ν_2-band profile at the band center ν_{fi} of the hot band in question, scaled by its vibrational

287 band intensity. Such simulations have been carried out for temperatures T of 1000, 2000, and

288 3000 K, respectively, and the results are shown in Figure 4(c), where they can be compared

289 to the experimental results[66,67] in Figure 4(b).

290 Figure 4 shows that the 'standard' $T = 300$ K rovibrational simulation of the CH$_3$ emis-

291 sion spectrum [Figure 4(a)] has little resemblance to the experimental spectrum from Ref.

292 66 [Figure 4(b)]. Obviously in the experiment, the CH$_3$ molecules populate states of much

293 higher energies than those accessed in thermal equilibrium at $T = 300$ K. However, among

294 the 'vibrational simulations' in Figure 4(c), the curve obtained for $T = 2000$ K has a very

295 substantial similarity to the experimental curve. This confirms the suggestion by Hermann

296 and Leone[66,67] that dissociation of CH_3I produces CH_3 radicals in highly excited states of

297 the out-of-plane bending mode ν_2. The successful simulation of the emission spectrum of

298 Refs. 66,67 lends credibility to the *ab initio* DMS of the present work; the intensities based

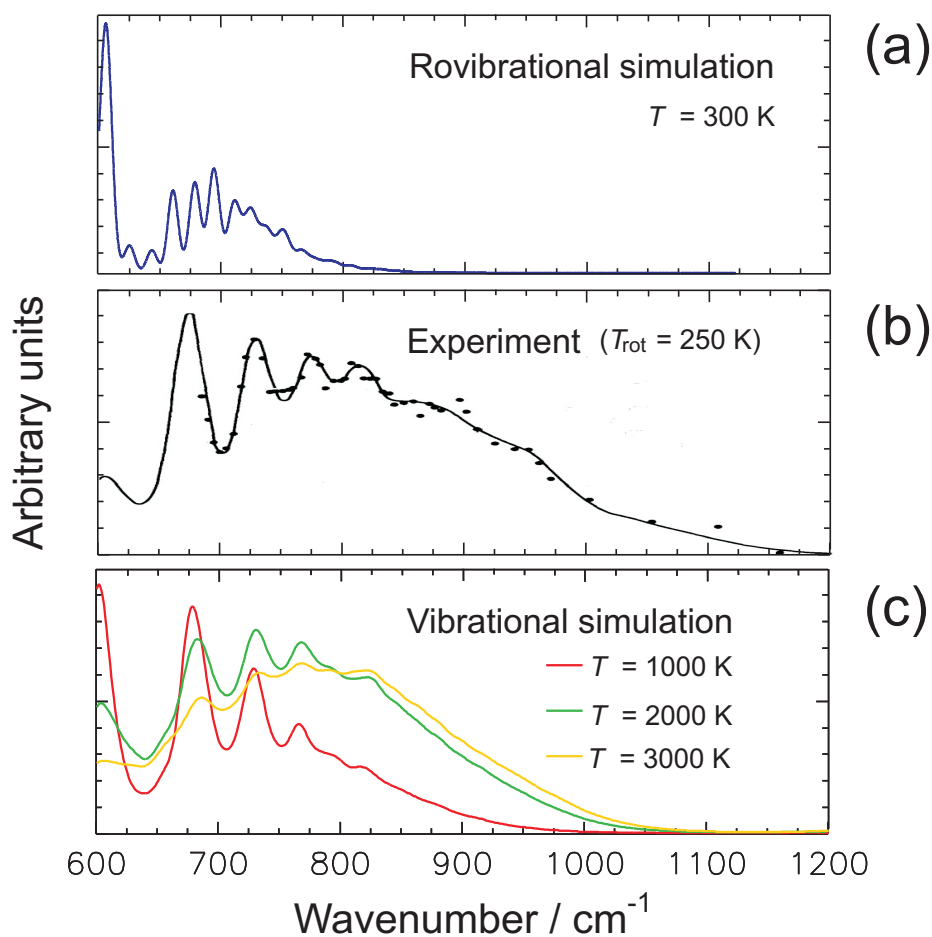299 on this DMS are in very good qualitative agreement with experiment.

300   Our complete $T = 1500$ K CH_3 line list is accessed via the repository `www.zenodo.org`,

301 see Ref. 68. It provides transition energies, line strengths, Einstein coefficients $A(f \leftarrow i)$ and

302 the temperature dependent partition function $Q(T)$. We expect the line list to be applicable

303 for temperatures below 1500 K. However, the simulated spectra will become increasingly

304 inaccurate with increasing temperature. The line list is given in the ExoMol format[20] which

305 can be used together with the ExoCross program[65] to generate spectra of CH_3.

Conclusion

306

307 We report here simulations of spectra for the methyl radical, extending over a significant

308 portion of the infrared spectral region. The positions and intensities calculated for the tran-

309 sitions are in excellent agreement with experiment, as demonstrated by detailed comparisons

310 with observed room-temperature spectra.

311   The CH_3 line list of the present work will facilitate detections of the methyl radical in

312 space. In the present work we have generated, refined, and validated the potential energy and

313 dipole moment surfaces required for the spectral simulations, and we have established the

314 level of accuracy attainable in variational nuclear-motion calculations with our computational

315 resources. We have produced a methyl radical line list consisting of 2 billion transitions

316 between 9,127,123 energy levels for ro-vibrational states up to $J_{\max} = 40$ and energies up to

317 19 000 cm^{-1}.

Figure 4: Emission spectra of CH_3. (a) Rovibrational simulation assuming the CH_3 radicals to be in thermal equilibrium at $T = 300$ K. (b) CH_3 (ν_2) out-of-plane bending mode emission spectrum (dots) obtained[66] after dissociation of $CH_3I \rightarrow CH_3(\nu_2) + I^*$. The continuous curve is the best fit[66] involving the hot bands $(v_2 + 1)\,\nu_2 \leftarrow v_2\,\nu_2$ with $v_2 \leqslant 9$. The spectrum is convolved with a spectrometer slit function with a FWHM of 33 cm^{-1} and a 19 cm^{-1} bandwidth ascribed to the breadth of the $\Delta K = 0$ manifold of transitions with varying J values. Reproduced from Ref. 66 with the permission of AIP Publishing. (c) Vibrational simulations at temperatures $T = 1000, 2000,$ and 3000 K, respectively, taking into account the vibrational transitions $(v_2 + 1)\,\nu_2 \leftarrow v_2\,\nu_2$ with $v_2 \leqslant 9$ (see text).

Acknowledgement

Supporting Information Available

The Supporting Information for this work includes: (i) dipole moment parameters $\mu^{(\Gamma)}_{k,l,m,...}$, (ii) potential energy parameters $f^{(s)}_{jk...}$; (iii) Fortran routines for calculating the dipole moment and potential energy values for a given geometry. Our complete $T = 1500K$ CH_3 line list together with the partition function can be accessed via the Zenodo repository, `www.zenodo.org`[68] as well as at `www.exomol.com`.

FIGURE CAPTIONS

332

333 Figure 1   Root-mean-square (RMS) errors of the fittings to the *ab initio* dipole moment

334   values. The results of a series of fittings are shown. In each fitting, the data

335   set includes the *ab initio* points with electronic energy (relative to the potential

336   energy minimum) $V \leqslant E$ (see text).

337 Figure 2   An overview of the absorption spectrum (cross sections) of CH_3 at different tem-

338   peratures $T = 300$, 500, 1000 and 1500 K generated using our line list and the

339   Gaussian line profile with the full-width-at-half-maximum of 1 cm^{-1}.

340 Figure 3   A selection of the strongest absorption bands of CH_3 at $T = 296$ K generated

341   using the line list. A Gaussian line profile with the half-width-half-maximum of

342   0.08 cm^{-1} was used in production of the cross sections shown.

343 Figure 4   Emission spectra of CH_3. (a) Rovibrational simulation assuming the CH_3 radicals

344   to be in thermal equilibrium at $T = 300$ K. (b) CH_3 (ν_2) out-of-plane bending

345   mode emission spectrum (dots) obtained[66] after dissociation of $CH_3I \to CH_3(\nu_2)$

346   + I*. The continuous curve is the best fit[66] involving the hot bands $(v_2 + 1)\,\nu_2 \leftarrow$

347               $v_2\,\nu_2$ with $v_2 \leqslant 9$. The spectrum is convolved with a spectrometer slit function

348   with a FWHM of 33 cm^{-1} and a 19 cm^{-1} bandwidth ascribed to the breadth of the

349               $\Delta K = 0$ manifold of transitions with varying J values. Reproduced from Fig. 4

350   of Ref. 66 with the permission of AIP Publishing. (c) Vibrational simulations at

351   temperatures $T = 1000$, 2000, and 3000 K, respectively, taking into account the

352   vibrational transitions $(v_2 + 1)\,\nu_2 \leftarrow v_2\,\nu_2$ with $v_2 \leqslant 9$ (see text).

References

(1) Miller, J. A.; Kee, R. J.; Westbrook, C. K. Chemical Kinetics and Combustion Modeling. *Annu. Rev. Phys. Chem.* **1990**, *41*, 345–387.

(2) Ravishankara, R. Kinetics of Radical Reactions in the Atmospheric Oxidation of CH_4. *Annu. Rev. Phys. Chem.* **1988**, *39*, 367–394.

(3) Jasinski, J. M.; Meyerson, B. S.; Scott, B. A. Mechanistic Studies of Chemical Vapor Deposition. *Annu. Rev. Phys. Chem.* **1987**, *38*, 109–140.

(4) Celii, F. G.; Butler, J. E. Diamond Chemical Vapor Deposition. *Annu. Rev. Phys. Chem.* **1991**, *42*, 643–684.

(5) Dmitriev, R. A. Z.; Dmitriev, Y. A. Detection of Free Radicals in Low-Temperature Gas-Grain Reactions of Astrophysical Interest. *Astron. Astrophys.* **2002**, *386*, 1129–1138.

(6) Feuchtgruber, H.; Moses, J. I.; Encrenaz, T. Detection of Methyl Radicals CH_3 on Saturn. *Astron. Astrophys.* **1998**, *44*, L41–L44.

(7) Bézard, B.; Romani, P. N.; Feuchtgruber, H.; Encrenaz, T. Detection of the Methyl Radical on Neptune. *Astrophys. J.* **1999**, *515*, 868–872.

(8) Feuchtgruber, H.; Helmich, F.; van Dishoeck, E. F.; Wright, C. M. Detection of Interstellar CH_3. *Astrophys. J.* **2000**, *535*, L111–L114.

(9) Settersten, T. B.; Farrow, R. L.; Gray, J. A. Coherent Infrared-Ultraviolet Double-Resonance Spectroscopy of CH_3. *Chem. Phys. Lett.* **2003**, *370*, 204–210.

(10) Lefohn, A. S.; Pimentel, G. C. Infrared Spectrum of Gaseous Methyl Radical by Rapid Scan Spectroscopy. *J. Chem. Phys.* **1972**, *57*, 4028–4037.

(11) Holt, P. L.; McCurdy, K. E.; Weisman, R. B.; Adams, J. S.; Engel, P. S. Transient CARS Spectroscopy of the ν_1 Band of Methyl Radical. *J. Chem. Phys.* **1984**, *81*, 3349–3350.

(12) Kelly, P. B.; Westre, S. G. Resonance Raman Spectroscopy of the Methyl Radical. *Chem. Phys. Lett.* **1988**, *151*, 253–257.

(13) Triggs, N. E.; Zahedi, M.; Nibler, J. W.; DeBarber, P.; Valentini, J. J. High Resolution Study of the ν_1 Vibration of CH_3 by Coherent Raman Photofragment Spectroscopy. *J. Chem. Phys.* **1992**, *96*, 1822–1831.

(14) Zahedi, M.; Harrison, J. A.; Nibler, J. W. 266 nm CH_3I Photodissociation: CH_3 Spectra and Population Distributions by Coherent Raman Spectroscopy. *J. Chem. Phys.* **1994**, *100*, 4043–4055.

(15) Hädrich, S.; Hefter, S.; Pfelzer, B.; Doerk, T.; Jauernik, P.; Uhlenbusch, J. Determination of the Absolute Raman Cross Section of Methyl. *Chem. Phys. Lett.* **1996**, *256*, 83–86.

(16) Westre, S. G.; Kelly, P. B. Examination of CD_3 Vibrational Structure by Resonance Raman Spectroscopy. *J. Chem. Phys.* **1989**, *90*, 6977–6979.

(17) Miller, J. T.; Burton, K. A.; Weisman, R. B.; Wu, W. X.; Engel, P. S. CARS Spectroscopy of Gas Phase CD_3. *Chem. Phys. Lett.* **1989**, *158*, 179–183.

(18) Adam, A. Y.; Yachmenev, A.; Yurchenko, S. N.; Jensen, P. Ro-Vibrational Averaging of the Isotropic Hyperfine Coupling Constant for the Methyl Radical. *J. Chem. Phys.* **2015**, *143*, 244306/1–7.

(19) Tennyson, J.; Yurchenko, S. N. ExoMol: Molecular Line Lists for Exoplanet and Other Atmospheres. *Mon. Not. R. Astron. Soc.* **2012**, *425*, 21–33.

(20) Tennyson, J.; Yurchenko, S. N.; Al-Refaie, A. F.; Barton, E. J.; Chubb, K. L.; Coles, P. A.; Diamantopoulou, S.; Gorman, M. N.; Hill, C.; Lam, A. Z. et al. The

ExoMol Database: Molecular Line Lists for Exoplanet and Other Hot Atmospheres. *J. Mol. Spectrosc.* **2016**, *327*, 73–94.

(21) Yurchenko, S. N.; Tennyson, J. ExoMol Line Lists IV: The Rotation-Vibration Spectrum of Methane Up to 1500 K. *Mon. Not. R. Astron. Soc.* **2014**, *440*, 1649–1661.

(22) Yurchenko, S. N.; Barber, R. J.; Yachmenev, A.; Thiel, W.; Jensen, P.; Tennyson, J. A Variationally Computed T=300 K Line List for NH_3. *J. Phys. Chem. A* **2009**, *113*, 11845–11855.

(23) Sousa-Silva, C.; Hesketh, N.; Yurchenko, S. N.; Hill, C.; Tennyson, J. High Temperature Partition Functions and Thermodynamic Data for Ammonia and Phosphine. *Journal of Quantitative Spectroscopy & Radiative Transfer* **2014**, *142*, 66–74.

(24) Sousa-Silva, C.; Al-Refaie, A. F.; Tennyson, J.; Yurchenko, S. N. ExoMol Line Lists - VII. The Rotation-Vibration Spectrum of Phosphine Up to 1500 K. *Mon. Not. R. Astron. Soc.* **2015**, *446*, 2337–2347.

(25) Underwood, D. S.; Yurchenko, S. N.; Tennyson, J.; Jensen, P. Rotational Spectrum of SO_3 and Theoretical Evidence for the Formation of Rotational Energy Level Clusters in its Vibrational Ground State. *J. Chem. Phys.* **2014**, *140*, 244316/1–10.

(26) Underwood, D. S.; Tennyson, J.; Yurchenko, S. N.; Clausen, S.; Fateev, A. ExoMol Line Lists XVII: A Line List for Hot SO_3. *Mon. Not. R. Astron. Soc.* **2016**, *462*, 4300–4313.

(27) Al-Refaie, A. F.; Yurchenko, S. N.; Yachmenev, A.; Tennyson, J. ExoMol Line Lists - VIII: A Variationally Computed Line List for Hot Formaldehyde. *Mon. Not. R. Astron. Soc.* **2015**, *448*, 1704–1714.

(28) Owens, A.; Yurchenko, S. N.; Yachmenev, A.; Tennyson, J.; Thiel, W. Accurate *ab initio* Vibrational Energies of Methyl Chloride. *J. Chem. Phys.* **2015**, *142*, 244306/1–10.

(29) Owens, A.; Yurchenko, S. N.; Yachmenev, A.; Thiel, W.; Tennyson, J. ExoMol Molecular Line Lists XXII. The Rotation-Vibration Spectrum of Silane Up to 1200 K. *Mon. Not. R. Astron. Soc.* **2017**, *471*, 5025–5032.

(30) Al-Refaie, A. F.; Ovsyannikov, R. I.; Polyansky, O. L.; Yurchenko, S. N.; Tennyson, J. A Variationally Calculated Room Temperature Line-List for H_2O_2. *J. Mol. Spectrosc.* **2015**, *318*, 84–90.

(31) Al-Refaie, A. F.; Polyansky, O. L.; Ovsyannikov, R. I.; Tennyson, J.; Yurchenko, S. N. ExoMol Line Lists XV: A Hot Line List for Hydrogen Peroxide. *Mon. Not. R. Astron. Soc.* **2016**, *461*, 1012–1022.

(32) Chubb, K. L.; Yachmenev, A.; Tennyson, J.; Yurchenko, S. N. Treating Linear Molecule HCCH in Calculations of Rotation-Vibration Spectra. *J. Chem. Phys.* **2018**, *149*, 014101/1–17.

(33) Mant, B. P.; Yachmenev, A.; Tennyson, J.; Yurchenko, S. N. ExoMol Molecular Line Lists - XXVII: Spectra of C_2H_4. *Mon. Not. R. Astron. Soc.* **2018**, *478*, 3220–3232.

(34) Gordon, I.; Rothman, L.; Hill, C.; Kochanov, R.; Tan, Y.; Bernath, P.; Birk, M.; Boudon, V.; Campargue, A.; Chance, K. et al. The HITRAN2016 Molecular Spectroscopic Database. *Journal of Quantitative Spectroscopy & Radiative Transfer* **2017**, *203*, 3 – 69, HITRAN2016 Special Issue.

(35) Bunker, P. R.; Jensen, P. *Molecular Symmetry and Spectroscopy*, 2nd ed.; NRC Research Press: Ottawa, 1998; p 748.

(36) Hudgens, J. W.; DiGiuseppe, T. G.; Lin, M. C. Two Photon Resonance Enhanced Multiphoton Ionization Spectroscopy and State Assignments of the Methyl Radical. *J. Chem. Phys.* **1983**, *79*, 571–582.

(37) Yamada, C.; Hirota, E. The Transition Dipole Moment of the ν_2 Band of the Methyl Radical. *J. Chem. Phys.* **1983**, *78*, 669–671.

(38) Wormhoudt, J.; McCurdy, K. E. A Measurement of the Strength of the ν_2 Band of CH_3. *Chem. Phys. Lett.* **1989**, *156*, 47–50.

(39) Stancu, G. D.; Röpcke, J.; Davies, P. B. Line Strengths and Transition Dipole Moment of the ν_2 Fundamental Band of the Methyl Radical. *J. Chem. Phys.* **2005**, *122*, 014306/1–11.

(40) Stancu, G. D.; Röpcke, J.; Davies, P. B. Measurement of the Transition Dipole Moment of the First Hot Band of the ν_2 Mode of the Methyl Radical by Diode Laser Spectroscopy. *J. Phys. Chem. A* **2008**, *112*, 6285–6288.

(41) Yurchenko, S. N.; Carvajal, M.; Jensen, P.; Lin, H.; Zheng, J.; Thiel, W. RotationVibration Motion of Pyramidal XY_3 Molecules Described in the Eckart Frame: Theory and Application to NH_3. *Mol. Phys.* **2005**, *103*, 359–378.

(42) Yurchenko, S. N.; Thiel, W.; Jensen, P. Theoretical ROVibrational Energies (TROVE): A Robust Numerical Approach to the Calculation of Rovibrational Energies for Polyatomic Molecules. *J. Mol. Spectrosc.* **2007**, *245*, 126–140.

(43) Yachmenev, A.; Yurchenko, S. N. Automatic Differentiation Method for Numerical Construction of the Rotational-Vibrational Hamiltonian as a Power Series in the Curvilinear Internal Coordinates Using the Eckart Frame. *J. Chem. Phys.* **2015**, *143*, 014105/1–16.

(44) Yurchenko, S. N.; Yachmenev, A.; Ovsyannikov, R. I. Symmetry-Adapted Rovibrational Basis Functions for Variational Nuclear Motion Calculations: TROVE Approach. *J. Chem. Theory Comput.* **2017**, *13*, 4368–4381.

(45) Adler, T. B.; Knizia, G.; Werner, H.-J. A Simple and Efficient CCSD(T)-F12 Approximation. *J. Chem. Phys.* **2007**, *127*, 221106/1–4.

(46) Adler, T. B.; Werner, H.-J. Local Explicitly Correlated Coupled-Cluster Methods: Efficient Removal of the Basis Set Incompleteness and Domain Errors. *J. Chem. Phys.* **2009**, *130*, 241101/1–5.

(47) Peterson, K. A.; Adler, T. B.; Werner, H.-J. Systematically Convergent Basis Sets for Explicitly Correlated Wavefunctions: The Atoms H, He, B-Ne, and Al-Ar. *J. Chem. Phys.* **2008**, *128*, 084102/1–12.

(48) Yachmenev, A.; Yurchenko, S. N.; Ribeyre, T.; Thiel, W. High-Level ab initio Potential Energy Surfaces and Vibrational Energies of H_2CS. *J. Chem. Phys.* **2011**, *135*, 074302.

(49) Lin, H.; Thiel, W.; Yurchenko, S. N.; Carvajal, M.; Jensen, P. Vibrational Energies for NH_3 Based on High Level *ab initio* Potential Energy Surfaces. *J. Chem. Phys.* **2002**, *117*, 11265–11276.

(50) Werner, H. J.; Knowles, P. J.; Knizia, G.; Manby, F. R.; Schütz, M. Molpro: A General-Purpose Quantum Chemistry Program Package. *Wiley Interdisciplinary Reviews: Computational Molecular Science* **2012**, *2*, 242–253.

(51) Watts, J. D.; Gauss, J.; Bartlett, R. J. Coupled-Cluster Methods with Noniterative Triple Excitations for Restricted Open-Shell Hartree–Fock and Other General Single Determinant Reference Functions. Energies and Analytical radients. *J. Chem. Phys.* **1993**, *98*, 8718–8733.

(52) Dunning, T. H. Gaussian Basis Sets for Use in Correlated Molecular Calculations. I. The Atoms Boron through Neon and Hydrogen. *J. Chem. Phys.* **1989**, *90*, 1007–1023.

(53) Kendall, R. A.; Dunning, Jr., T. H.; Harrison, R. J. Electron Affinities of the First-Row Atoms Revisited. Systematic Basis Sets and Wave Functions. *J. Chem. Phys.* **1992**, *96*, 6796–6806.

(54) Yurchenko, S. N.; Carvajal, M.; Lin, H.; Zheng, J.; Thiel, W.; Jensen, P. Dipole Moment and Rovibrational Intensities in the Electronic Ground state of NH_3: Bridging the Gap Between *ab initio* Theory and Spectroscopic Experiment. *J. Chem. Phys. 122*, 104317/1–14.

(55) Yurchenko, S. N.; Thiel, W.; Carvajal, M.; Lin, H.; Jensen, P. Rotation-Vibration Motion of Pyramidal XY3 Molecules Described in the Eckart Frame: The Calculation of Intensities with Application to NH_3. *Adv. Quantum Chem.* **2005**, *48*, 209–238.

(56) Bunker, P. R.; Jensen, P. *The Fundamentals of Molecular Symmetry*, 1st ed.; CRC Press: Boca Raton, 2004; p 358.

(57) Špirko, V.; Bunker, P. R. The Potential Function and Rotation-Vibration Energy Levels of the Methyl Radical CH_3. *J. Mol. Spectrosc.* **1982**, *95*, 381–390.

(58) Davis, S.; Anderson, D. T.; Duxbury, G.; Nesbitt, D. J. Jet-Cooled Molecular Radicals in Slit Supersonic Discharges: Sub-Doppler Infrared Studies of Methyl Radical. *J. Chem. Phys.* **1997**, *107*, 5661–5675.

(59) Al-Refaie, A. F.; Yurchenko, S. N.; Tennyson, J. GPU Accelerated Intensities MPI GAIN-MPI: A New Method of Computing Einstein-A Coefficients. *Comput. Phys. Commun.* **2017**, *214*, 216–224.

(60) Ovsyannikov, R. I.; Thiel, W.; Yurchenko, S. N.; Carvajal, M.; Jensen, P. Vibrational Energies of PH_3 Calculated Variationally at the Complete Basis Set Limit. *J. Chem. Phys.* **2008**, *129*, 044309/1–8.

(61) Yamada, C.; Hirota, E.; Kawaguchi, K. Diode Laser Study of the ν_2 Band of the Methyl Radical. *J. Chem. Phys.* **1981**, *75*, 5256–5264.

(62) Jacox, M. E. *Vibrational and Electronic Energy Levels of Polyatomic Transient Molecules. Supplement B*; American Chemical Society: New York, 2005; Vol. 1.

(63) Bethardy, G. A.; Macdonald, R. G. Direct Measurement of the Transition Dipole Moment of the ν_3 Asymmetric C-H Stretching Vibration of the CH_3 Radical. *J. Chem. Phys.* **1995**, *103*, 2863–2872.

(64) Tanarro, I.; Sanz, M. M.; Domingo, C.; Bermejo, D.; Santos, J.; Domenech, J. L. Transition Dipole Moment of the ν_3 Band of CH_3. *J. Phys. Chem.* **1994**, *98*, 5862–5866.

(65) Yurchenko, S. N.; Al-Refaie, A. F.; Tennyson, J. ExoCross: A General Program for Generating Spectra from Molecular Line Lists. *Astron. Astrophys.* **2018**, *614*, A131/1–12.

(66) Hermann, H. W.; Leone, S. R. Photofragment Infrared Emission Spectroscopy: Vibrational Progression and Potential Parameters of the $CH_3(\nu_2)$ Umbrella" Mode. *J. Chem. Phys.* **1982**, *76*, 4759–4765.

(67) Hermann, H. W.; Leone, S. R. Photofragmentation Dynamics of CH_3I at 248 and 266 nm: Vibrational Distributions in the $CH_3(\nu_2)$ Umbrella" Mode. *J. Chem. Phys.* **1982**, *76*, 4766–4774.

(68) Adam, A. Y.; Yachmenev, A.; Yurchenko, S. N.; Jensen, P. Supplementary Material: A Variationally Computed IR Line List for the Methyl Radical CH_3. 2019; Zenodo. https://doi.org/10.5281/zenodo.2607732.

1
2
3
4
5
6
7
8
9
10
11
12
13
14
15
16
17
18
19
20
21
22
23
24
25
26
27
28
29
30
31
32
33
34
35
36
37
38
39
40
41
42
43
44
45
46
47
48
49
50
51
52
53
54
55
56
57
58
59
60

534

535

TOC graphics